Helmholtz Free Energy Equation of State for ^3He–^4He Mixtures at Temperatures Above 2.17 K

Cite as: J. Phys. Chem. Ref. Data **50**, 043102 (2021); https://doi.org/10.1063/5.0056087
Submitted: 06 May 2021 • Accepted: 07 September 2021 • Published Online: 06 October 2021

Changzhao Pan, Haiyang Zhang, Gérard Rouillé, et al.

Journal of Physical and Chemical Reference Data | ARTICLE | scitation.org/journal/jpr

Helmholtz Free Energy Equation of State for ^{3}He–^{4}He Mixtures at Temperatures Above 2.17 K

Cite as: J. Phys. Chem. Ref. Data 50, 043102 (2021); doi: 10.1063/5.0056087
Submitted: 6 May 2021 • Accepted: 7 September 2021 •
Published Online: 6 October 2021

Changzhao Pan,[1,2,a)] Haiyang Zhang,[2,3,a)] Gérard Rouillé,[4] Bo Gao,[2,3] and Laurent Pitre[1,2]

AFFILIATIONS

[1] Laboratoire National de métrologie et d'Essais-Conservatoire National des Arts et Métiers (LNE-CNAM), 93210 La Plaine-Saint Denis, France
[2] TIPC-LNE Joint Laboratory on Cryogenic Metrology Science and Technology, Technical Institute of Physics and Chemistry (TIPC), Chinese Academy of Sciences (CAS), Beijing 100190, China
[3] CAS Key Laboratory of Cryogenics, Technical Institute of Physics and Chemistry, Chinese Academy of Sciences, Beijing 100190, China
[4] Institut d'Astrophysique Spatiale (IAS), Université Paris Saclay, 91405 Orsay CEDEX, France

[a)] **Authors to whom correspondence should be addressed:** changzhao.pan@lecnam.net and zhy110@mail.ipc.ac.cn

ABSTRACT

The work presents the first wide-range equation of state (EOS) for ^{3}He–^{4}He mixtures based on the reduced Helmholtz free energy multi-fluid approximation model. It covers the temperature range from 2.17 to 300 K and the pressure from the vapor pressure up to 3 MPa for any given mixture ^{3}He mole fraction. In this model, the ^{4}He and ^{3}He reduced Helmholtz free energy equations and departure functions from the literature are employed and only five unknown mixture parameters are needed for each given departure function. The parameters and the best model for the concerned binary mixture were determined by the Levenberg–Marquardt optimization method. With the best developed model, the liquid, gaseous, and saturated thermophysical properties of the mixture can be mostly described with an accuracy better than 5%. Furthermore, a database for the thermophysical properties of ^{3}He–^{4}He mixtures is generated and provided for interpolation in temperature, pressure, and ^{3}He mole fraction. The current EOS and database can be applied to the design and optimization of ultra-low temperature refrigerators.

Key words: dilution refrigerator; equation of state; ^{3}He–^{4}He mixtures; Helmholtz free energy; pulse-tube cryocooler; space cryogenic; vapor-liquid equilibrium.

CONTENTS

List of Tables

List of Figures

1. Introduction

Since the first liquefaction of ^{4}He in 1908[1] and the discovery of the superfluidity of pure ^{3}He in 1971,[2] the fascination for understanding the properties of ^{3}He–^{4}He quantum fluids at ultra-low temperatures has not ended. The ideal Fermi gas model of ^{3}He–^{4}He solutions was first proposed by Landau and Pomeranchuk[3] and improved by Bardeen *et al.*,[4] Radebaugh,[5] and Kuerten *et al.*[6] Those calculations were restricted to zero pressure, ^{3}He mole fractions below 8%, and temperatures below 250 mK. Extending these efforts, Chaudhry *et al.*[7,8] published the thermodynamic properties of liquid ^{3}He–^{4}He mixtures over the entire composition range between 0.15 and 1.5 K and up to 10 bars. At higher temperatures, Karnatsevich *et al.*[9] developed an empirical equation of state (EOS) for equimolar ^{3}He–^{4}He mixtures in the temperature range 1.5–14 K by using an expression close to the EOS for ^{4}He proposed by McCarty.[10] Sibileva *et al.*[11] improved the empirical EOS for the liquid phase over the whole fraction range. However, there is still no unified EOS for ^{3}He–^{4}He mixtures covering a wide range of temperature, pressure, and composition.

The efforts made by Chaudhry *et al.*[7,8] were to develop sub-kelvin refrigeration cycles that use ^{3}He–^{4}He mixtures as the working fluid, which could prove to be more efficient than ^{3}He–^{4}He dilution refrigerators by eliminating many of the losses associated with the latter.[12] These newer cycles use mixtures of ^{3}He and ^{4}He with much higher fractions of ^{3}He.[13] The proper design of these machines requires knowledge of ^{3}He–^{4}He mixture properties over the entire fraction range from pure ^{3}He to pure ^{4}He and up to temperatures in excess of 1.2 K, a natural choice for the high-temperature reservoir for a sub-kelvin refrigerator.

Efficient refrigeration from 300 to 1.2 K is the other part of such efforts and is our motivation. Low frequency (less than 2 Hz) pulse-tube refrigeration offers unprecedented reliability with no moving parts in the cold end, together with cryogen-free operation up to 20 000 h before standard maintenance.[14] Using ^{4}He as the working fluid, the lowest temperature of a pulse-tube refrigerator is limited by the alpha line of pure ^{4}He at 2.17 K.[15–17] Indeed, the base temperature of a commercial ^{4}He pulse-tube refrigerator is 2.5 K. Lower temperature to about 1.3 K can be achieved by replacing ^{4}He with ^{3}He.[18] However, the price and availability of ^{3}He limit its large-scale application as a pure gas.[19] An alternative solution is the use of ^{3}He–^{4}He mixtures. Figure 1 shows the phase diagram of ^{3}He–^{4}He mixtures at different pressures and the alpha line [the ideal cooling power for a pulse-tube cryocooler is $\dot{Q} = T\alpha_v V_m \overline{\dot{n} \cdot \delta p}$, as shown in Eq. (5) in Ref. 19, so it only works in the region of $\alpha_v > 0$] ($\alpha_v = 0$, where α_v is the volumetric thermal expansion coefficient, whose expression can be found in Sec. 3.3) of the ^{3}He–^{4}He mixture. One may note that with a 60% ^{3}He mole fraction, temperatures below 1.2 K may be achieved. This can be compared with the usual 25% mole fraction used for dilution refrigeration. Among our motivations, we aim to introduce a new efficient and reliable ^{3}He–^{4}He 300–1 K Vuilleumier Pulse-Tube Cooler (VPTC) for the space cooling chains of sub-kelvin refrigerators.[21,22] This effort would allow reducing the cold mass of present cooling chains by almost half. This would be a breakthrough since the cold mass of a sub-kelvin cooler including redundancy may be by weight about one third of the satellite mass.

Up until now, we have shown that the thermodynamic properties of ^{3}He–^{4}He mixtures are well documented above the superfluid transition temperature of ^{3}He at 2.44 mK and 34.3 MPa, up to 14 K. However, there is still no EOS for ^{3}He–^{4}He gaseous mixtures for a wide range of ^{3}He mole fractions, allowing the calculation of all thermodynamic properties required for designing 1 K class cryocoolers.

In recent years, Kunz and Wagner[23,24] published the GERG-2008 mixture model with an EOS based on the Helmholtz free energy, which may be applied to binary mixtures. In this model, the Helmholtz free energy is expressed as an explicit function of density, temperature, and composition, from where all the other thermophysical properties can be accurately derived. We use this model to build the first EOS for the ^{3}He–^{4}He binary mixture using the Helmholtz free energy EOS for pure ^{3}He[25] and ^{4}He[26,27] and construct the first wide-range EOS for ^{3}He–^{4}He mixtures from 2.17 K to room temperature and from the vapor pressure to pressures higher than 3 MPa.

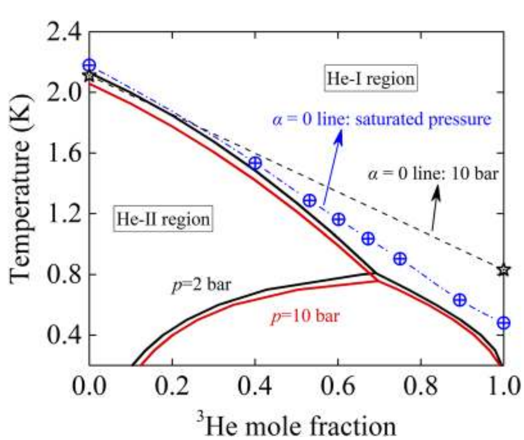

FIG. 1. The ^{3}He–^{4}He mixture phase diagram at the pressures of 2 and 10 bars and the $\alpha = 0$ line at saturated pressure (the phase-separation curve at high pressure is from Ref. 8, and the $\alpha = 0$ line is from Ref. 20).

The remainder of this paper is structured as follows. In Sec. 2, the database used in the present work is summarized. In Sec. 3, the theoretical model is described in detail, in which the fundamental equation, thermophysical property calculation method, and optimization method are presented. In Sec. 4, the fitting results and the fitting error are presented. Finally, a conclusion in Sec. 5 completes the paper.

2. Database

2.1. Critical parameters

The critical parameters for pure ^{3}He and ^{4}He have been well studied by many researchers. In the present work, the critical parameters in Refs. 25 and 27 are used, as shown in Table 1. For the critical temperature of the ^{3}He–^{4}He mixture, its value depends on the ^{3}He mole fraction. One can find experimental data for the critical temperature of ^{3}He–^{4}He mixtures in the work of Wallace and Meyer.[30]

2.2. Vapor–liquid equilibrium properties

The available experimental data for vapor–liquid equilibrium (VLE) properties of ^{3}He–^{4}He mixtures are summarized in Table 2, which includes the bubble-point pressure, the dew-point pressure, the saturated vapor density, and the saturated liquid density at temperatures above 2.17 K. Eselson and Berezniak[28] measured the bubble-point and dew-point pressures in a wide range of ^{3}He mole fraction from 0.04 to 0.908 in the temperature range from 1.2 to 3.5 K. Wallace *et al.*[30,29] measured the bubble-point and dew-point pressures in a range of ^{3}He mole fraction from 0.2 to 0.886 at temperatures up to the critical temperature. Sydoriak and Roberts[31] and Sreedhar and Daunt[32] measured the bubble-point pressure in the range of ^{3}He mole fraction from 0.1 to 0.9 at temperatures below 2.4 K and from 0.01 to 0.12 at temperatures below 2.6 K, respectively. Sibilyova *et al.*[33] presented the bubble-point pressure with a ^{3}He mole fraction of 0.4 in the temperature range from 2.25 to 3.75 K.

For the saturated density, Ptukha[34] measured saturated liquid density in a wide range of ^{3}He mole fractions from 0.1 to 0.85 in the temperature range from 1.3 to 3.9 K. Eselson *et al.*[35] measured saturated liquid density with ^{3}He mole fraction from 0 to 1 at temperatures from 1.4 to 4.2 K. Sibilyova *et al.*[36] presented saturated vapor and liquid density with ^{3}He mole fractions of 0.2, 0.6, and 0.8 in the temperature range from 2.25 to 4.2 K. Wang *et al.*[37] measured saturated liquid density with ^{3}He mole fraction from 0 to 0.5 at temperatures from 1.3 to 4.4 K. However, those data were only found after the fitting, so they are only used for checking the performance of the developed EOS in this work.

2.3. ρpT data and virial coefficients

The only two ρpT experimental data sources for ^{3}He–^{4}He mixtures are the works of Bogoyavlensky *et al.*,[38,39] as shown in

TABLE 1. The molar mass and critical parameters for pure ^{4}He and ^{3}He

	M (g/mol)	T_c (K)	p_c (MPa)	ρ_c (mol/m^3)
^{3}He[25]	3.016 03	3.315 7	0.114 603 9	41.191
^{4}He[27]	4.002 602	5.195 3	0.227 46	69.58

TABLE 2. The database of the VLE properties for ^{3}He–^{4}He mixtures

Sources	Points	T (K)	p (MPa)	x	Uncertainty
		Saturated pressure			
Eselson and Bereznia[28]	140	2.17–3.2	0.007–0.05	0.04–0.908	0.5% in bubble pressure 2%–3% in dew-point pressure
Wallace and Meyer[30]	94[a]	2.2–4.8	0.006–0.17	0.2–0.866	0.5%
Wallace *et al.*[29]	20	2.5–3.0	0.004–0.07	0.2–0.866	0.5%
Sydoriak and Roberts[31]	18	<2.4	0.008–0.02	0.1–0.9	1% in x
Sreedhar and Daunt[32]	20	<2.6	0.006–0.018	0.02–0.12	1.2% in vapor pressure
Sibilyova *et al.*[33]	7	2.25–3.75	0.016–0.11	0.4	⋯
		Saturated density			
Ptukha[34]	49	2.18–3.9	Saturated	0.1–0.85	1%[b]
Eselson *et al.*[35]	62	2.2–4.2	Saturated	0–1	⋯
Wallace *et al.*[29]	20	2.5–3.0	Saturated	0.2–0.866	0.5%
Sibilyova *et al.*[36]	46	2.25–4.2	Saturated	0.2–0.8	$T < 3$ K, 3% $T > 3$ K, 6%
Wang *et al.*[37]	84	2.2–4.4	Saturated	0–0.494	0.2% in saturated density

[a]There are no tabular data in the reference, so we selected some data points along the smooth curve in the figure.
[b]Systematic error.

Table 3. Those data cover temperatures up to 4.2 K and pressures up to 2.4 MPa for the liquid-phase region and temperatures up to 20 K and pressures up to 3.6 MPa for the gaseous region in a wide range of ^{3}He mole fraction. Besides ρpT data, the virial coefficient is also important for an EOS. Keller[40] and Karnatsevic *et al.*[42] reported experimental data for the second virial coefficients for ^{3}He–^{4}He mixtures. Barrufet and Eubank[41] reported the second virial coefficients for ^{3}He–^{4}He mixtures at temperatures below 5 K derived from the ρpT data of Wallace and Meyer.

TABLE 3. The database of ρpT data and virial coefficients for ^{3}He–^{4}He mixtures

Sources	Points	T (K)	p (MPa)	x	Uncertainty
		ρpT			
Bogoyavlensky and Yuechenko[38]	432	2.25–4.2	0.1–2.4	0.352–0.651	0.1% in x 0.2% in p 0.2% in ρ
Bogoyavlensky *et al.*[39]	1499	4.5–20.2	0.03–3.6	0–1	0.1% in x 0.2% in p 10 mK in T 0.2%–3% in ρ
		Second virial coefficient			
Keller[40]	2	2.2–4		0.5475	⋯
Wallace and Meyer[a]	45	3.55–5		0.2–0.8	⋯
Karnatsevic *et al.*[42]	35	4.48–8.9		0–1	⋯
Hurly and Moldover[43]	75	1–10 000		0.5	⋯
Cencek *et al.*[44]	79	1–10 000		0.5	0.001%–2.36%

[a]The original reference is Wallace and Meyer, “Tabulation of the original pressure-volume-temperature data for ^{3}He-^{4}He mixtures and for ^{3}He,” A technical report from the Department of Physics, Duke University, 1984, but this technical report cannot be found. Here, the data are taken from Ref. 41 that refers to the above report.

Hurly and Moldover[43] presented the second virial coefficients for equimolar ^{3}He–^{4}He mixtures using *ab initio* calculation. However, the uncertainty of those calculations is not clear. Cencek *et al.*[44] presented the interaction virial B_{34} for ^{3}He–^{4}He mixtures with very small uncertainty, which can be used to calculate the second virial coefficients at any given ^{3}He mole fraction.

2.4. Heat capacity and sound speed

The heat capacity and sound speed can be calculated from the second derivative of the Helmholtz free energy EOS, so they are also important for the fitting of EOS. Table 4 summarizes those data. Dokoupil *et al.*[45] measured saturated heat capacity with ^{3}He mole fraction from 0 to 0.417 at temperatures up to 4 K. Pandorf *et al.*[46] measured heat capacity at constant volume near the freezing pressure with ^{3}He mole fraction from 0.17 to 0.95 at temperatures up to 4.5 K. For sound speed, the main data are from the work of Vignos and Fairbank,[47] who measured the sound speed of ^{3}He–^{4}He mixtures with ^{3}He mole fractions of 0.25, 0.75, and 0.98 at pressures up to 7 MPa and temperatures up to 4.5 K. The data from the work of Roberts and Sydoriak[48] and Eselson *et al.*[49] were only found after our fitting was complete, so they are only used for checking the performance of the EOS developed in this work.

3. Fundamental Equation and Fitting Process

3.1. Multi-fluid approximations model

The EOS for ^{3}He–^{4}He mixtures used in the present work is explicitly expressed as the reduced Helmholtz free energy α, which includes an ideal part α^0 and a residual part α^r,[23,24]

$$\alpha(\delta,\tau,\boldsymbol{x}) = \frac{a(\rho,T,\boldsymbol{x})}{RT} = \alpha^0(\rho,T,\boldsymbol{x}) + \alpha^\mathrm{r}(\delta,\tau,\boldsymbol{x}), \tag{1}$$

where a is the Helmholtz free energy and ρ, T, and $\boldsymbol{x}$ are the density, temperature, and mole fraction vector of mixture components. R is the universal gas constant. Since 20 May 2019, all SI units are defined in terms of constants that describe the natural world. The Boltzmann constant is fixed as $k = 1.380\,649 \times 10^{-23}$ J K^{-1}, and the Avogadro constant is fixed as $N_\mathrm{A} = 6.022\,140\,76 \times 10^{23}$ mol^{-1}.[50] Then, R is fixed as $R = kN_\mathrm{A} = 8.314\,462\,618$ J mol^{-1} K^{-1}.

δ and τ are the reduced mixture density and inverse reduced mixture temperature, which are defined as

$$\delta = \frac{\rho}{\rho_\mathrm{r}} \text{ and } \tau = \frac{T_\mathrm{r}}{T}, \tag{2}$$

where ρ_r and T_r are the composition-dependent reducing functions for the mixture density and temperature, respectively. The GERG-2008 reducing functions were used in the present work, which have been widely used as the mixing rule for various refrigerant mixtures.[24] Their formulations are

$$T_\mathrm{r}(\boldsymbol{x}) = \sum_{i=1}^{N} x_i^2 T_{\mathrm{c},i} + \sum_{i=1}^{N}\sum_{j=2}^{N} 2x_i x_j \beta_{T,ij}\gamma_{T,ij}\frac{x_i + x_j}{\beta_{T,ij}^2 x_i + x_j} \times (T_{\mathrm{c},i}\cdot T_{\mathrm{c},j})^{0.5}, \tag{3}$$

$$\frac{1}{\rho_\mathrm{r}(\boldsymbol{x})} = \sum_{i=1}^{N} x_i^2 \frac{1}{\rho_{\mathrm{c},i}} + \sum_{i=1}^{N}\sum_{j=2}^{N} 2x_i x_j \beta_{v,ij}\gamma_{v,ij}\frac{x_i + x_j}{\beta_{v,ij}^2 x_i + x_j} \times \left(\frac{1}{\rho_{\mathrm{c},i}^{1/3}} + \frac{1}{\rho_{\mathrm{c},j}^{1/3}}\right)^3, \tag{4}$$

where the parameter γ is symmetric and parameter β is asymmetric; then, there are four parameters ($\beta_{T,12}$, $\gamma_{T,12}$, $\beta_{v,12}$, $\gamma_{v,12}$) that need to be fitted.

The ideal gas part and residual part of the reduced Helmholtz free energy for the mixtures are functions of the pure-fluid Helmholtz free energies, which can be expressed as

$$\alpha^0(\rho,T,\boldsymbol{x}) = \sum_{i=1}^{N} x_i\left[\alpha_{\mathrm{o}i}^0(\rho,T) + \ln x_i\right], \tag{5}$$

$$\alpha^\mathrm{r}(\delta,\tau,\boldsymbol{x}) = \sum_{i=1}^{N} x_i \alpha_{\mathrm{o}i}^\mathrm{r}(\delta,\tau) + \Delta\alpha^\mathrm{r}(\delta,\tau,\boldsymbol{x}), \tag{6}$$

where $\alpha_{\mathrm{o}i}^0$ is the ideal part of the reduced Helmholtz free energy of pure ^{3}He and ^{4}He and $\alpha_{\mathrm{o}i}^\mathrm{r}$ is the residual part of the reduced Helmholtz free energy of pure ^{3}He and ^{4}He. The pure helium Helmholtz free energies will be introduced in detail in Sec. 3.2.

TABLE 4. The database of heat capacity and speed of sound for ^{3}He–^{4}He mixtures

Sources	Points	T (K)	p (MPa)	x	Uncertainty
		Heat capacity			
Dokoupil *et al.*[45]	40[a]	2.2–4	Saturated	0.01–0.417	4%
Pandorf *et al.*[46]	49[a]	2.5–4.5	5–15	0.17–0.95	⋯
		Sound speed			
Vignos and Fairbank[47]	122	2.5–4	0.1–7	0.25–0.98	0.1%–0.3% in w
Roberts and Sydoriak[48]	2	2.2–2.3	Saturated	0.301	0.3% in w
Eselson *et al.*[49]	43	2.5–4.2	Saturated	0–0.2	0.05% in x 0.15% in w

[a]Data points selected from the smooth curve in the figure.

TABLE 5. Departure function coefficients for the KW0 model[24]

k	N_k	d_k	t_k	l_k	η_k	ε_k	β_k	γ_k
1	2.557 477 684 411 8	1	1	0	0	0	0	0
2	−7.984 635 713 635 3	1	1.55	0	0	0	0	0
3	4.785 913 146 580 6	1	1.7	0	0	0	0	0
4	−0.732 653 924 000 0	2	0.25	0	0	0	0	0
5	1.380 547 134 531 2	2	1.35	0	0	0	0	0
6	0.283 496 035 000 0	3	0	0	0	0	0	0
7	−0.490 873 859 000 0	3	1.25	0	0	0	0	0
8	−0.102 918 889 000 0	4	0	0	0	0	0	0
9	0.118 363 147 000 0	4	0.7	0	0	0	0	0
10	0.000 055 527 385 7	4	5.4	0	0	0	0	0

$\Delta\alpha^{\mathrm{r}}$ is the departure function for the multicomponent mixtures. It is used to describe the non-ideal behavior of mixtures,

$$\Delta\alpha^{\mathrm{r}}(\delta,\tau,\boldsymbol{x}) = \sum_{i=1}^{N-1}\sum_{j=i+1}^{N} x_i x_j F_{ij}\alpha_{ij}^{\mathrm{r}}(\delta,\tau), \tag{7}$$

where F_{ij} is the interaction parameter for the binary mixture, which is the fifth parameter to be fitted in the present work. α_{ij}^{r} is the departure function for the binary pair. In the present work, the purpose is to build a reliable and practical Helmholtz free energy EOS for ^{3}He–^{4}He mixtures covering the limited available data. The equation is based on the thermodynamic relation between the concerned properties and the reduced Helmholtz free energy (for details, see Sec. 3.3). Due to the limited available literature data for this binary mixture, we built the Helmholtz free energy EOS in the common way,[51,52] i.e., only optimizing the five parameters by using published and accepted departure functions (using four departure functions can give a check for the fitting quality and sensitivity of the departure function) [hydrocarbon mixtures in GERG 2008 (called KW0 later)[24] and departure functions for ^{4}He–Ne, ^{4}He–Ar, and Ne–Ar[53]] and then comparing the four different combinations to better describe the thermophysical properties of the ^{3}He–^{4}He binary mixture. The formulation of the departure function for KW0 is in Eq. (8), and its coefficients are given in Table 5. The formulation of the departure function for ^{4}He–Ne, ^{4}He–Ar, and Ne–Ar is the same as in Eq. (9), and the coefficients of those departure functions are given in Table 6,

$$\alpha_{ij}^{\mathrm{r}}(\delta,\tau) = \sum N_k\delta^{d_k}\tau^{t_k}\exp\Big(-\mathrm{sgn}(l_k)\cdot\delta^{l_k} - \eta_k(\delta-\varepsilon_k)^2 - \beta_k(\delta-\gamma_k)^2\Big), \tag{8}$$

$$\alpha_{ij}^{\mathrm{r}}(\delta,\tau) = \sum N_k\delta^{d_k}\tau^{t_k}\exp\Big(-\mathrm{sgn}(l_k)\cdot\delta^{l_k} - \eta_k(\delta-\varepsilon_k)^2 - \beta_k(\tau-\gamma_k)^2\Big). \tag{9}$$

3.2. Helmholtz free energy EOS for pure helium

To build an accurate EOS for ^{3}He–^{4}He mixtures, a high-accuracy Helmholtz free energy EOS for pure helium is required. For ^{4}He, its Helmholtz free energy EOS has been well developed[26,27] and widely used in software such as REFPROP.[54] It can be expressed as[27]

TABLE 6. Departure function coefficients for ^{4}He mixtures[53]

k	N_k	t_k	d_k	η_k	β_k	γ_k	ε_k
			^{4}He–Ne				
1	−4.346 85	1.195	1	0	0	0	0
2	−0.884 38	1.587	2	0	0	0	0
3	0.258 416	1.434	3	0	0	0	0
4	3.502 188	1.341	1	−0.157	−0.173	1.31	1.032
5	0.831 33	1.189	2	−0.931	−1.07	1.356	1.978
6	2.740 495	1.169	3	−0.882	−0.695	1.596	1.966
7	−1.582 23	0.944	4	−0.868	−0.862	1.632	1.709
8	−0.304 9	1.874	4	−0.543	−0.971	0.766	0.583
			^{4}He–Ar				
1	−2.643 65	1.03	1	0	0	0	0
2	−0.347 5	0.288	2	0	0	0	0
3	0.201 207	0.572	3	0	0	0	0
4	1.171 326	1.425	1	−0.371	−0.32	1.409	0.378
5	0.216 379	1.987	1	−0.081	−1.247	1.709	0.741
6	0.561 37	0.024	2	−0.375	−1.152	0.705	0.322
7	0.182 57	1.434	3	−0.978	−0.245	1.162	1.427
8	0.017 879	0.27	4	−0.971	−1.03	0.869	2.088
			Ne–Ar				
1	−1.039 69	0.723	1	0	0	0	0
2	0.593 776	1.689	2	0	0	0	0
3	−0.186 53	1.365	3	0	0	0	0
4	−0.223 32	0.201	1	−1.018	−0.36	1.119	2.49
5	0.160 847	0.164	2	−0.556	−0.373	1.395	1.202
6	0.405 228	0.939	2	−0.221	−0.582	1.01	2.468
7	−0.264 56	1.69	3	−0.862	−0.319	1.227	0.837
8	−0.033 57	1.545	4	−0.809	−0.56	1.321	2.144

$$\alpha_{\mathrm{o}}^{0}(\delta,\tau) = \ln\frac{\rho_{\mathrm{r}}}{\rho_{\mathrm{c}}}\delta + (a_0-1)\ln\frac{T_{\mathrm{c}}}{T_{\mathrm{r}}}\tau + a_1 + a_2\frac{T_{\mathrm{c}}}{T_{\mathrm{r}}}\tau, \tag{10}$$

$$\alpha_{\mathrm{o,He_4}}^{\mathrm{r}}(\delta,\tau) = \sum_1^k N_k\delta^{d_k}\tau^{t_k} \times\exp\Big(-\mathrm{sgn}(l_k)\cdot\delta^{l_k} - \eta_k(\delta-\varepsilon_k)^2 - \beta_k(\tau-\gamma_k)^2\Big), \tag{11}$$

where $a_0 = 2.5$, $a_1 = 0.173\,348\,642\,2$, and $a_2 = 0.467\,452\,363\,8$ for ^{4}He. T_{c} and ρ_{c} are the critical temperature and density, as shown in Table 1. N_k, d_k, t_k, l_k, η_k, ε_k, β_k, and γ_k are the coefficients and exponents for ^{4}He. The values of these parameters are shown in Table 7. The model has a very good performance on the density and speed of sound with errors less than 0.5%, and the error of heat capacity is about 2%.

^{3}He has not been widely studied and does not have a reference formulation like ^{4}He. The most accurate ^{3}He Helmholtz free

TABLE 7. The Helmholtz free energy EOS coefficients and exponents for ^{4}He (Ref. 27)

k	N_k	t_k	d_k	l_k	η_k	β_k	γ_k	ε_k
1	0.015 559	1	4	0	0	0	0	0
2	3.063 893	0.425	1	0	0	0	0	0
3	−4.242 08	0.63	1	0	0	0	0	0
4	0.054 418	0.69	2	0	0	0	0	0
5	−0.189 72	1.83	2	0	0	0	0	0
6	0.087 856	0.575	3	0	0	0	0	0
7	2.283 357	0.925	1	1	0	0	0	0
8	−0.533 32	1.585	1	2	0	0	0	0
9	−0.532 97	1.69	3	2	0	0	0	0
10	0.994 449	1.51	2	1	0	0	0	0
11	−0.300 79	2.9	2	2	0	0	0	0
12	−1.643 26	0.8	1	1	0	0	0	0
13	0.802 91	1.26	2	0	1.5497	0.2471	3.15	0.596
14	0.026 839	3.51	1	0	9.245	0.0983	2.54505	0.3423
15	0.046 877	2.785	2	0	4.76323	0.1556	1.2513	0.761
16	−0.148 33	1	1	0	6.3826	2.6782	1.9416	0.9747
17	0.030 162	4.22	1	0	8.7023	2.7077	0.5984	0.5868
18	−0.019 99	0.83	3	0	0.255	0.6621	2.2282	0.5627
19	0.142 835	1.575	2	0	0.3523	0.1775	1.606	2.5346
20	0.007 418	3.447	2	0	0.1492	0.4821	3.815	3.6763
21	−0.229 9	0.73	3	0	0.05	0.3069	1.61958	4.5245
22	0.792 248	1.634	2	0	0.1668	0.1758	0.6407	5.039
23	−0.049 39	6.13	2	0	42.2358	1357.658	1.076	0.959

energy was developed based on Debye phonon theory by Huang *et al.*,[25] which has been used in the software He3Pak[55] and REGEN.[56] This Debye model is valid from 0.01 K to room temperature with pressures from the vapor pressure to the melting pressure. The ρpT, heat capacity, and sound speed calculated by this model have a good accuracy with errors within 1%, except the error of heat capacity in the gaseous phase region, which is up to 6.32%. The Helmholtz free energy based on the Debye model is expressed as[25]

$$a_{\mathrm{He}_3}(\delta,1/\tau) = -\Theta H_0 + \frac{1}{1+\mathrm{e}^{C_1(1/\tau-1)}}\sum_{i=1}^{4}\frac{\delta^i\left(C_{2i+5}(1/\tau)^2 + C_{2i+6}(1/\tau)^4\right)}{1+\mathrm{e}^{iC_2(\delta-1)}} + \sum_{i=1}^{3}C_{i+14}\delta^i + \sum_{i=1}^{2}\left[\frac{\delta^i}{1+\mathrm{e}^{C_3(\delta-1)}}\left(C_{2i+16} + C_{2i+17}\frac{1}{1+\mathrm{e}^{C_4(1/\tau-1)}}\right)\right]$$
$$+ \frac{\left(1-\mathrm{e}^{-C_5/\tau}\right)^2}{1+\mathrm{e}^{C_6(1/\delta-1)}}\sum_{i=1}^{4}\left[(C_5/\tau)^{i-3}\left(C_{3i+19} + C_{3i+20}\delta + C_{3i+21}\delta^2\right)\right] - C_{34}/\tau + C_{35}, \tag{12}$$

where Θ is the Debye theta and ΘH_0 is the ideal Helmholtz free energy from the basic Debye phonon theory. In the present work, the values of coefficients C_i take the same value as in the software REGEN 3.3, as shown in Table 8. One also needs to be careful in changing the form of Eq. (12), especially when using its derivative to calculate the other thermophysical properties. To be convenient, the Appendix shows the changes of its derivative.

In order to develop the Helmholtz free energy EOS for mixtures, Eq. (12) is rewritten as the ideal part and reduced part like ^{4}He. To be convenient, the same ideal part of the reduced Helmholtz free energy [same as Eq. (10)] is used for pure ^{3}He, and the residual part of the reduced Helmholtz free energy can be expressed as

$$\alpha^{\mathrm{r}}_{\mathrm{o},\mathrm{He}_3}(\delta,\tau) = \frac{\tau}{RT_{\mathrm{c}}}a_{\mathrm{He}_3}(\delta,1/\tau) - \alpha^0_{\mathrm{o}}(\delta,\tau). \tag{13}$$

3.3. Thermodynamic properties from Helmholtz free energy

From the above reduced Helmholtz free energy of ^{3}He–^{4}He mixtures, all the other thermodynamic properties can be calculated, as shown in Table 9 (which only presents the main properties for analyzing cryocoolers; one can find all the others in Ref. 24). However, in the practical application, because the pressure is more easily measured than density, pressure is usually used as the

TABLE 8. The Helmholtz free energy EOS coefficients for ^3He (Refs. 25 and 56)

C_{1-10}	C_{11-20}	C_{21-30}	C_{31-38}
2.671 780 514	1.312 844 165	4.881 756 64	0.028 348 498
0.991 964 789	−2.259 725 062	0.917 917 318	−0.396 573 697
2.296 872 88	−0.459 896 431	−6.583 662 879	0.061 367 227
2.584 609 302	0.715 119 974	1.273 447 716	7.815 876 899
0.110 712 677	−0.873 794 229	2.153 080 193	6.729 311 6
0.236 350 211	−2.663 910 299	−6.662 204 915	3.272 801 522
2.859 386 169	1.071 179 613	1.282 675 91	0.304 642 607
−1.453 876 695	−2.347 570 003	0.833 196 39	0.061 983 903
−4.341 750 761	−2.574 785 443	−2.290 583 478	0
3.168 840 649	−0.029 477 671	0.366537464	0

input parameter instead of density. To obtain the value of density, the Newton–Raphson method can be used to solve the pressure equation in Table 9. The detailed solution process can be found in Ref. 52.

In addition to the above thermodynamic properties, VLE properties can provide more input data, which help obtain the optimal fitting parameters. From the reduced Helmholtz free energy of ^3He–^4He mixtures, the VLE can be obtained by solving the equilibrium conditions

$$\begin{cases} T_{\text{liquid}} = T_{\text{vapor}}, \\ p_{\text{liquid}} = p_{\text{vapor}}, \\ f_{\text{liquid},i} = f_{\text{vapor},i}, \end{cases} \tag{14}$$

where f is the fugacity of component i, which can be calculated from the fugacity coefficient[52]

$$\ln(\varphi_i) = \alpha^{\text{r}} + \delta\alpha^{\text{r}}_{\delta} - \ln\left(1 + \delta\alpha^{\text{r}}_{\delta}\right) + (1 - x_i)\left(-\frac{\delta\alpha^{\text{r}}_{\delta}}{\rho_{\text{r}}}\frac{\partial\rho_{\text{r}}}{\partial x_i} + \frac{\tau\alpha^{\text{r}}_{\tau}}{T_{\text{r}}}\frac{\partial T_{\text{r}}}{\partial x_i} + \alpha^{\text{r}}_{x_i}\right). \tag{15}$$

There are several methods that can be used to solve the equilibrium conditions. Here, the common Newton–Raphson method is used.[57] One can find other methods in the literature.[58,59] By solving the equilibrium conditions using the reduced Helmholtz free energy of ^3He–^4He mixtures, the bubble-point pressure, dew-point pressure, saturated liquid density, and saturated vapor density of ^3He–^4He mixtures can be obtained.

3.4. Optimization method

In the above model, the unknown five parameters are the four binary parameters ($\beta_{T,12}$, $\gamma_{T,12}$, $\beta_{v,12}$, $\gamma_{v,12}$) in Eqs. (3) and (4) and the interaction parameter (F_{12}) in Eq. (7). As mentioned before, four departure functions (KW0, ^4He–Ne, ^4He–Ar, and Ne–Ar) were tested. For each of them, the departure function coefficients were fixed and the unknown five parameters, $\beta_{T,12}$, $\gamma_{T,12}$, $\beta_{v,12}$, $\gamma_{v,12}$, F_{12}, were optimized with the Levenberg–Marquardt method. The goal is to minimize the residual sum of squares of calculated and experimental data, and the objective function can be written as

$$\chi^2 = \frac{1}{N_c}\sum W_c\left(\frac{C_{v,\text{cal}} - C_{v,\text{exp}}}{C_{v,\text{exp}}}\right)^2 + \frac{1}{N_w}\sum W_w\left(\frac{w_{\text{cal}} - w_{\text{exp}}}{w_{\text{exp}}}\right)^2 + \frac{1}{N_p}\sum W_p\left(\frac{p_{\text{cal}} - p_{\text{exp}}}{p_{\text{exp}}}\right)^2 + \frac{1}{N_\rho}\sum W_\rho\left(\frac{\rho_{\text{cal}} - \rho_{\text{exp}}}{\rho_{\text{exp}}}\right)^2, \tag{16}$$

where N is the total number of experimental data, W is a weighting coefficient, C_v is the isochoric heat capacity, w is the speed of sound,

TABLE 9. The thermodynamic properties derived from the reduced Helmholtz free energy

Property	Relation to α	Property	Relation to α
Pressure	$\frac{p}{\rho RT} = 1 + \delta\alpha^{\text{r}}_{\delta}$	Compression factor	$Z = 1 + \delta\alpha^{\text{r}}_{\delta}$
Internal energy	$\frac{u}{RT} = \tau\left(\alpha^0_\tau + \alpha^{\text{r}}_\tau\right)$	Enthalpy	$\frac{h}{RT} = 1 + \tau\left(\alpha^0_\tau + \alpha^{\text{r}}_\tau\right) + \delta\alpha^{\text{r}}_{\delta}$
Isochoric heat capacity	$\frac{C_v}{R} = -\tau^2\left(\alpha^0_{\tau\tau} + \alpha^{\text{r}}_{\tau\tau}\right)$	Speed of sound	$\frac{Mw^2}{RT} = 1 + 2\delta\alpha^{\text{r}}_{\delta} + \delta^2\alpha^{\text{r}}_{\delta\delta} + \frac{\left(1+\delta\alpha^{\text{r}}_{\delta}-\delta\tau\alpha^{\text{r}}_{\delta\tau}\right)^2}{\tau^2\left(\alpha^0_{\tau\tau}+\alpha^{\text{r}}_{\tau\tau}\right)}$
Isobaric heat capacity	$\frac{C_p}{R} = -\tau^2\left(\alpha^0_{\tau\tau} + \alpha^{\text{r}}_{\tau\tau}\right) + \frac{\left(1+\delta\alpha^{\text{r}}_{\delta}-\delta\tau\alpha^{\text{r}}_{\delta\tau}\right)^2}{1+2\delta\alpha^{\text{r}}_{\delta}+\delta^2\alpha^{\text{r}}_{\delta\delta}}$	Volumetric thermal expansion coefficient	$\alpha_v T = \frac{\left(1+\delta\alpha^{\text{r}}_{\delta}-\delta\tau\alpha^{\text{r}}_{\delta\tau}\right)}{\left(1+2\delta\alpha^{\text{r}}_{\delta}+\delta^2\alpha^{\text{r}}_{\delta\delta}\right)}$

TABLE 10. Optimized parameters and objective function values for ^3He–^4He mixtures

	$\beta_{T,12}$	$\gamma_{T,12}$	$\beta_{v,12}$	$\gamma_{v,12}$	F_{12}	χ^2
KW0	1.010 348 12	1.013 693 13	1.012 189 49	0.977 416 78	0.059 846 8	0.061 8
^4He–Ar	1.017 886 12	1.001 223 20	1.029 022 11	0.974 895 06	0.001 569 35	0.068 5
Ne–Ar	1.026 592 40	1.003 488 58	1.018 375 17	0.975 521 68	0.005 208 43	0.075 8
^4He–Ne	1.030 465 95	1.002 108 03	1.016 524 58	0.985 061 54	0.003 342 57	0.091 7

TABLE 11. The average absolute relative deviations of different departure functions (the bold font numbers indicate the best; the italic numbers indicate the worst)

	KW0	^{4}He–Ne	^{4}He–Ar	Ne–Ar
	AARD (%)			
C_v	**3.245**	*4.191*	3.873	3.941
w	*1.218*	**1.149**	1.193	1.216
p_{bubble}	**3.763**	5.214	*5.884*	5.220
p_{dew}	**2.398**	*2.962*	2.624	2.712
$\rho_{\text{sat,l}}$	0.967	1.103	*1.413*	**0.963**
$\rho_{\text{sat,v}}$	*5.106*	4.601	4.629	**4.014**
p_{l}	**2.704**	3.691	*3.820*	2.757
ρ_{l}	**0.329**	*0.420*	0.357	0.331
p_{g}	**1.469**	*1.964*	1.644	1.630
ρ_{g}	**1.212**	*1.327*	1.219	1.213

and p and ρ include the pressure and density at gaseous, liquid, and VLE states. Because the heat capacity from Ref. 45 is at the saturated state, it was not used in the fitting process and only used to check the performance of the developed EOS. In the optimization process, to improve the convergence, the VLE data are first fitted and then the gaseous and liquid data are added to improve the fitting parameters.

Finally, the performances of fitting results are evaluated by the average absolute relative deviation, which is defined as

$$AARD = \frac{100}{N}\sum_{i=1}^{N}\left|\frac{X_{\text{cal}} - X_{\text{exp}}}{X_{\text{exp}}}\right|, \tag{17}$$

where X represents the property from the literature and N is the total number of data points of X. The subscripts cal and exp denote the calculated and experimental values of property X.

4. Results and Discussion

Based on the above method, an optimization code was written using the MATLAB software. The optimized parameters and objective function values of different departure functions are shown in Table 10. One can see that the KW0 model shows the minimum calculated objective function values among the four models used. To further evaluate the effectiveness of each departure function, the average absolute relative deviations for different thermophysical properties are shown in Table 11. Bold and italic fonts are used to indicate the minimum and maximum deviation values of different models. One can see that the KW0 model performs better on the heat capacity and all the pressures, but it is a little worse for the saturated density calculation. The Ne–Ar model gives a medium outcome among the different models. The ^{4}He–Ne and ^{4}He–Ar models are not as good as the others, but all the average absolute relative deviations are within 6%.

4.1. Deviation from experimental data

Figures 2 and 3 show the calculated isotherms in the gaseous and liquid phase region. The experimental data cover a range of temperatures from 4.52 to 13 K with pressures from 0.03 to 3.6 MPa for gas and from 2.25 to 4.2 K with pressures from 0.1 to 2.4 MPa for liquid. One can see that the calculated results are very consistent with the experimental data. For the gaseous state results at 4.52 K, the calculated isothermal line with ^{3}He mole fractions of 0.1708 and 0.3518 can also predict the behavior of the gas–liquid transition near the critical region.

The fitting residuals of all the ρpT isothermal data are shown in Fig. 4. One can see that the residuals are well within 1% for the liquid region. For the gaseous region data, most residuals are within 2%, but for the data at low pressure, especially near the critical region, the residual could be higher than 4%.

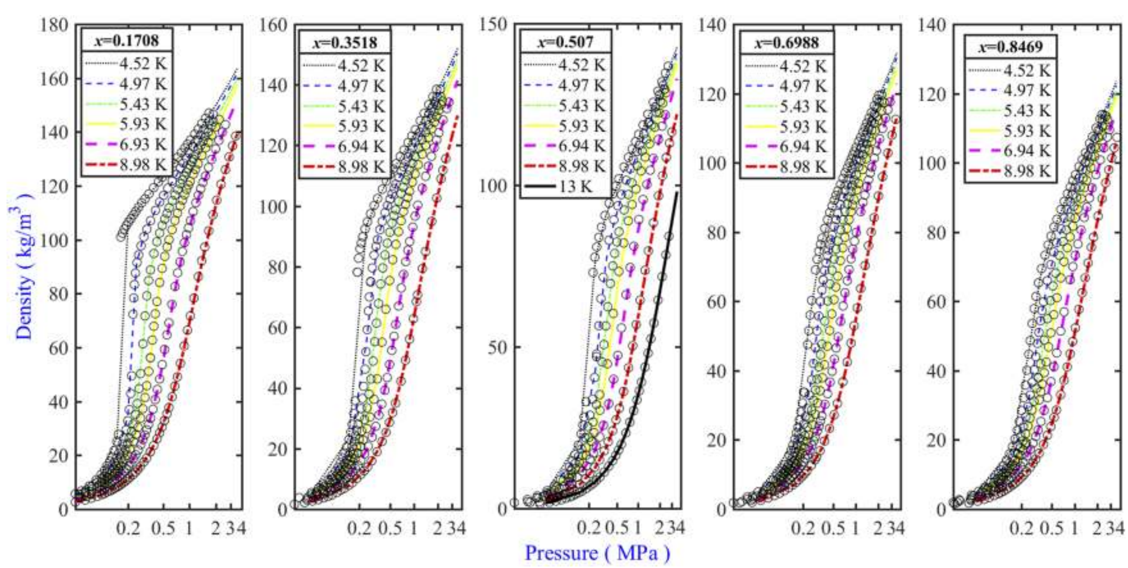

FIG. 2. Comparison of the calculated isotherms (KW0 model) with the experimental data[39] in the gaseous region. Circles are experimental data; the lines and dashed lines are calculated data. The x-axis is a logarithmic coordinate to clearly show the low-pressure data.

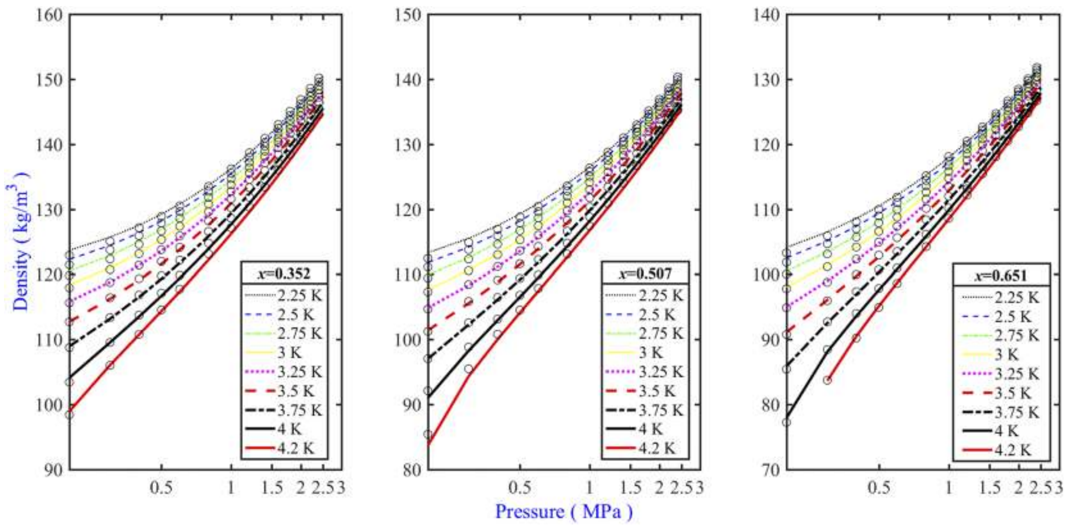

FIG. 3. Comparison of the calculated isotherms with the experimental data[38] in the liquid region. Circles are experimental data; the lines and dashed lines are calculated data. The x-axis is a logarithmic coordinate to clearly show the low-pressure data.

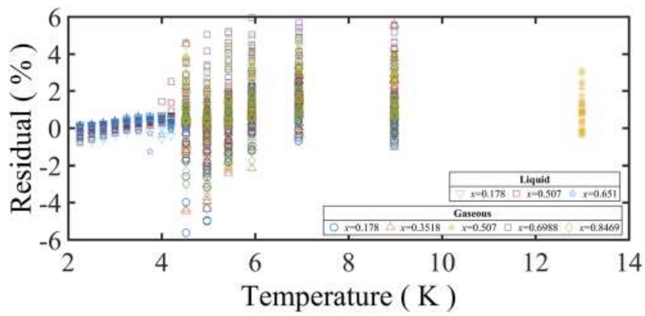

FIG. 4. The fitting residuals of all the ρpT isothermal data.

Figure 5 shows the x = 0.507 isobaric line in the gaseous phase region. It covers a range of temperatures from 4.3 to 20.2 K and pressures from 0.1 to 1.61 MPa. One can see that the calculated results from the EOS developed in the present work are consistent with the experimental data. Here, experimental data at temperatures from 4.35 to 4.99 K at 0.195 MPa from Ref. 39 are not used because those points are too close to the two-phase region and the calculation model is unable to predict them.

Figures 6–9 show comparisons of calculated VLE properties with experimental data from the literature.[28–36] One can see that the present EOS can also predict well most of the VLE properties. The errors of calculated saturated liquid density and bubble-point pressure are as good as 2%, except for points near the critical region where the errors of calculated bubble-point pressure increase to above 5%. The errors of calculated dew-point pressure show a little higher error of 5%, mainly because the experimental data have a larger uncertainty. However, for the saturated gas density, the present EOS shows relatively poor prediction in which the calculation errors increase up to 8%.

As mentioned before, the saturated liquid density data from Ref. 37 were only found after the optimization of the five parameters given in Table 10. Figure 10 shows the comparison of the molar volume between the present EOS and the data of Wang *et al.*[37]

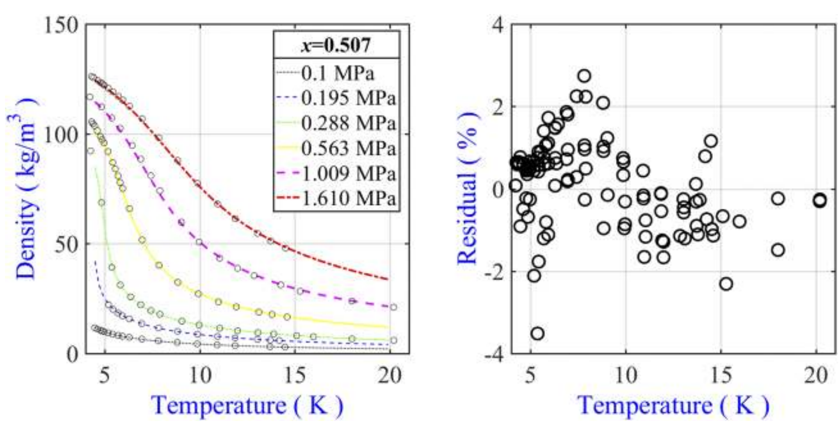

FIG. 5. Comparison of the calculated isobaric line in the gaseous region using the KW0 model with the experimental data[39] and its residuals. Circles are experimental data; the lines and dashed lines are calculated data.

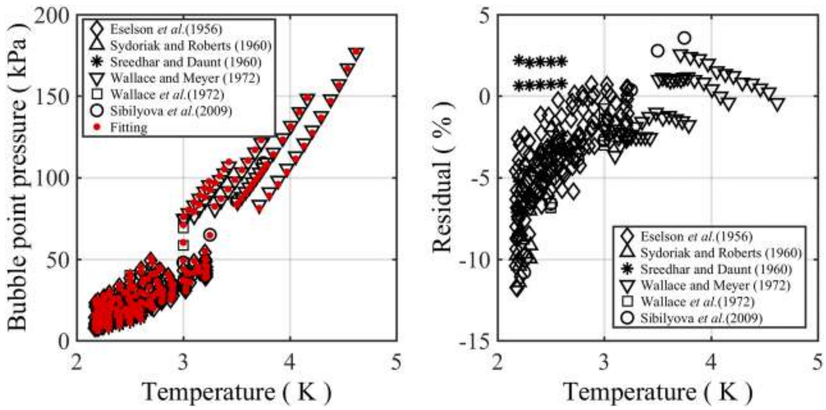

FIG. 6. Comparison of the calculated vapor pressure using the KW0 model with the experimental data[28–33] and its residuals.

The present results show excellent agreement with the experimental data, and the deviation is generally less than 1%.

Figures 11 and 13 compare the calculated isochoric and saturated heat capacity with the experimental data from the literature.[45,46] The available experimental data are limited to isochoric heat capacities at high pressure near the solidification region and saturated heat capacity at the saturated state. Most isochoric heat capacity data can be predicted with an accuracy of 5%, as shown in Fig. 12. However, for the predicted saturated heat capacity [the saturated heat capacity is the heat capacity along the saturation line, which can be calculated from the equation $C_{\mathrm{sat}} = C_p - T\frac{\mathrm{d}V}{\mathrm{d}T}\left(\frac{\mathrm{d}P}{\mathrm{d}T}\right)_{\mathrm{sat}}$], the present EOS has a predictive trend with

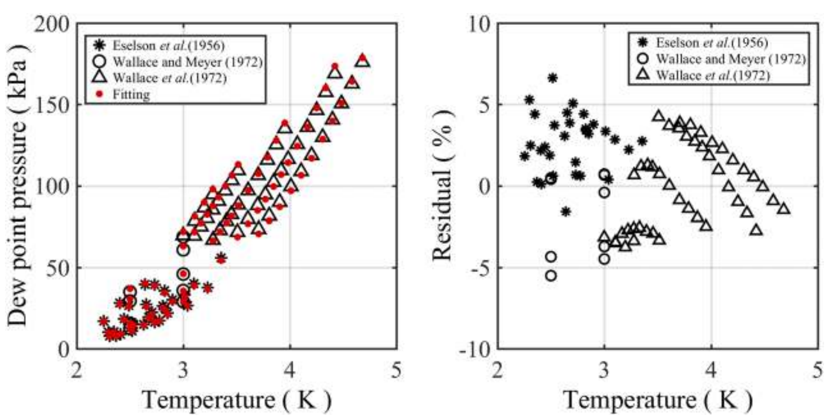

FIG. 7. Comparison of the calculated dew-point pressure using the KW0 model with the experimental data[28–29] and its residuals.

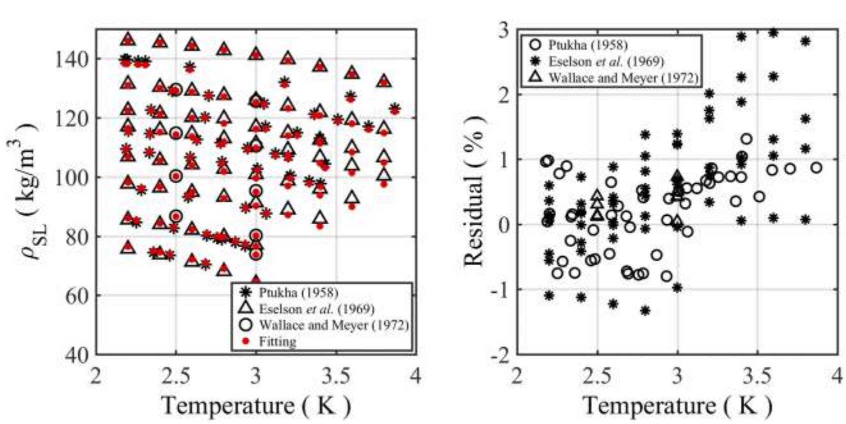

FIG. 8. Comparison of the calculated saturated liquid density using the KW0 model with the experimental data[30,34,35] and its residuals.

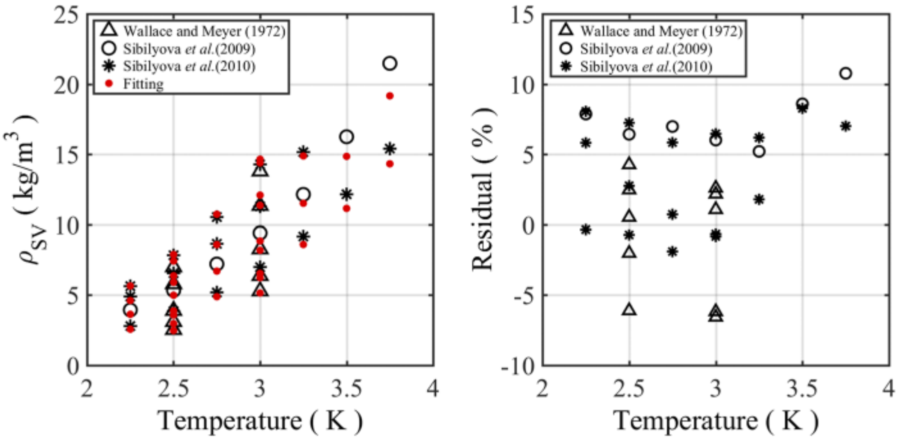

FIG. 9. Comparison of the calculated saturated vapor density using the KW0 model with the experimental data[30,33,36] and its residuals.

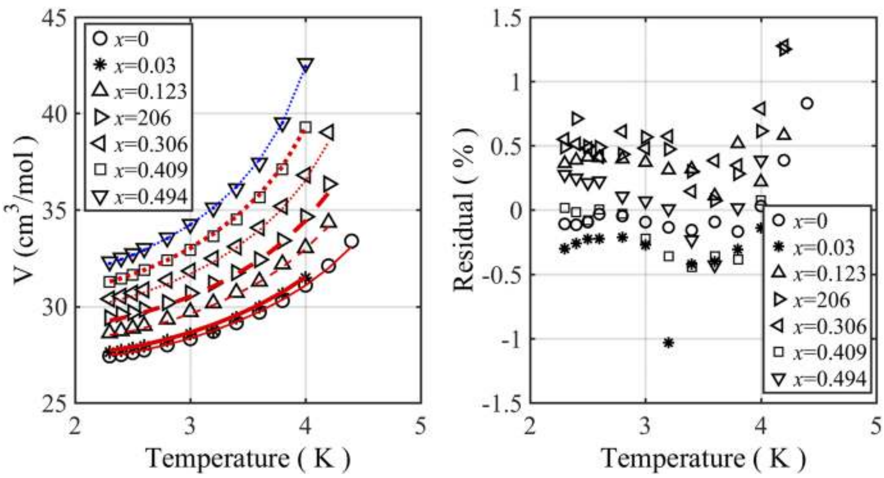

FIG. 10. Comparison of the calculated molar volume using the KW0 model with the experimental data[37] and its residuals. The line and dashed line are the calculated data.

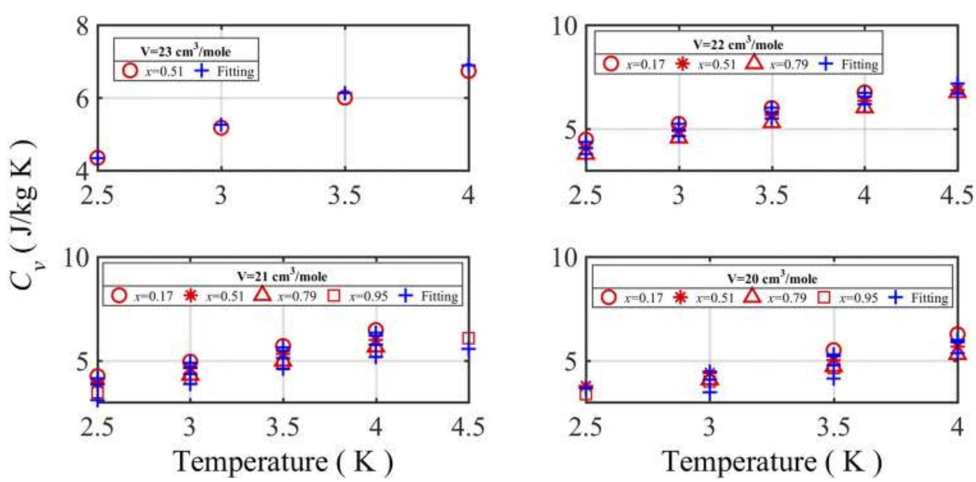

FIG. 11. Comparison of the calculated isochoric heat capacity using the KW0 model with the experimental data at four molar volumes.[46]

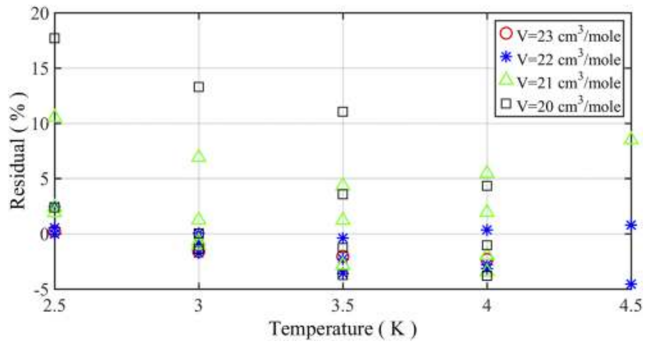

FIG. 12. The fitting residuals of all the C_v data.

the maximum error higher than 10%, as shown in Fig. 13. There are two reasons for the weak prediction of saturated heat capacity. One is the Helmholtz free energy model for pure ^{3}He, whose maximum error for heat capacity can be as high as 6.32%. The second reason is that the experimental data of the heat capacity are at the saturated state with a relatively large uncertainty of about 4%. In the calculation, one needs first to obtain the saturated density and then to calculate the heat capacity, which also increases the calculated error. In the future, more accurate experimental data for heat capacity are needed to check and improve the present EOS.

Figures 14 and 15 compare the calculated sound speed in the liquid mixture and the experimental data from Ref. 47. In the wide ^{3}He mole fraction range of 0.25–0.98 and pressures from 0.1 to 7 MPa, the present EOS has a good prediction with errors within 2%. Table 12 presents the comparison results of the two calculated speeds of sound at vapor pressure with experimental data from Ref. 48. It is evident that the present model can also predict the speed of sound well at the vapor pressure with an accuracy around 1%. In addition, the present calculated sound speeds at the saturated liquid state are compared with the experimental results from Ref. 49, as shown in Fig. 16. The residual errors are better than 3%. The data from REFPROP software for pure ^{4}He are also compared in Fig. 16; one can see that the data from Ref. 49 also deviate from the REFPROP values.

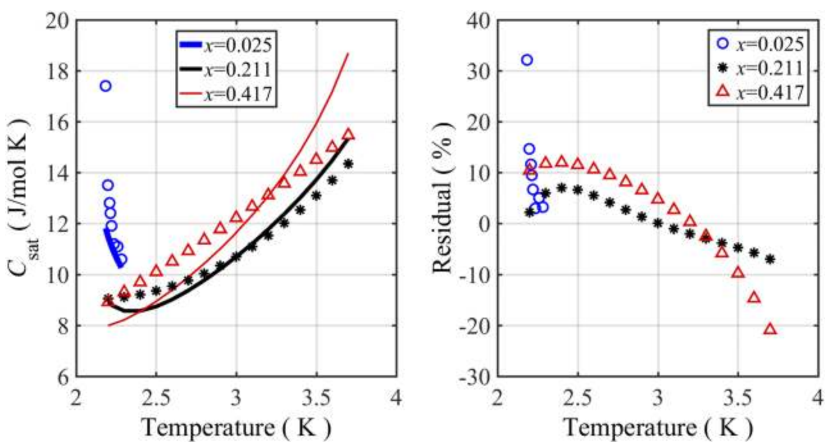

FIG. 13. Comparison of the calculated isochoric heat capacity using the KW0 model with the experimental data.[45] The solid lines are the calculated data.

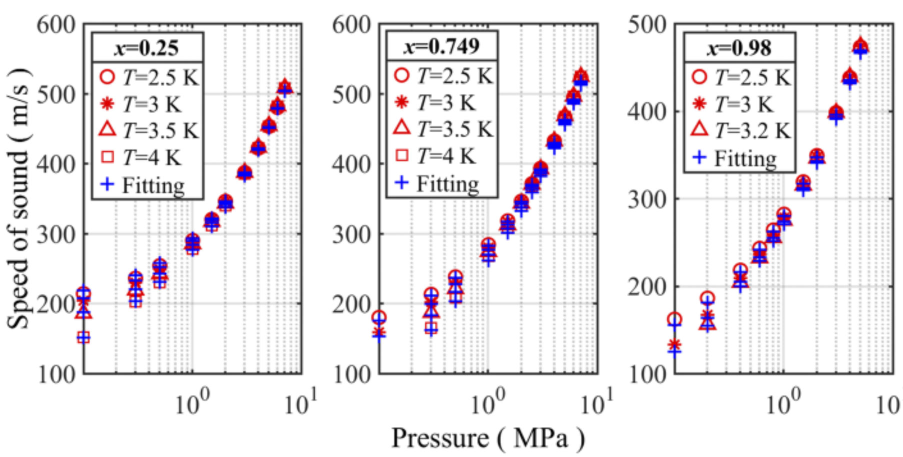

FIG. 14. Comparison of the calculated speed of sound using the KW0 model with the experimental data.[47]

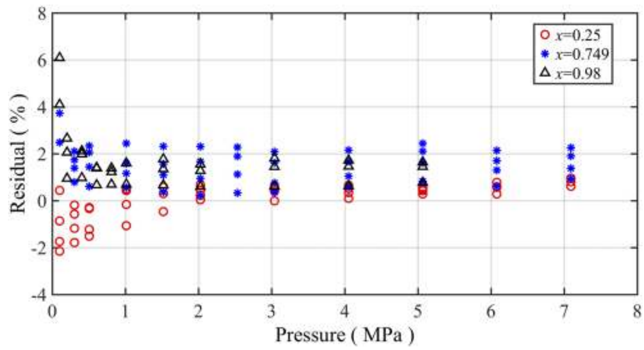

FIG. 15. The fitting residuals of all the sound-speed data.

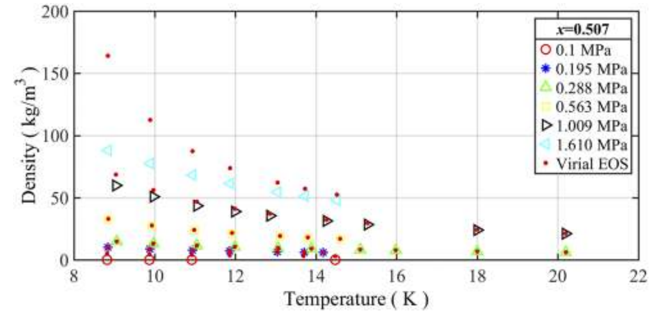

FIG. 17. Comparison of the calculated density using the virial EOS (only using second virial coefficient) with the experimental data from Ref. 39.

TABLE 12. Comparison of the calculated isochoric heat capacity using the KW0 model with the experimental data[48]

T (K)	x	w_{exp} (m/s)	w_{cal} (m/s)	Error (%)
2.305	0.301	203.33	205.40	1.02
2.206	0.301	204.34	205.24	0.44

4.2. Extrapolation of the present EOS to T above 20 K

From the above comparisons, one can see that the present EOS shows good prediction of the ρpT relation at temperatures below 20 K. However, for practical application, the ^{3}He–^{4}He mixture normally works from room temperature to the low temperature. We found no experimental data for ^{3}He–^{4}He mixtures at temperatures above 20 K. In order to check the present EOS at a higher temperature, a feasible way is to compare it with the virial EOS (VEOS). VEOS is a well-known EOS that is a polynomial series in the density, is explicit in pressure, and can be derived from statistical mechanics,[60]

$$\frac{p}{\rho RT} = 1 + B(T)\rho + C(T)\rho^2 + \cdots,$$

where $B(T)$, $C(T)$, . . ., are the second, third, . . ., virial coefficients. For ^{3}He–^{4}He mixtures, the second virial coefficient has been accurately computed by Hurly and Moldover[43] and Cencek *et al.*[44] using *ab initio* calculation, and there are no available data for the third or higher order mixture virial coefficients. Because the calculated interaction virial B_{34} for ^{3}He–^{4}He mixtures from Ref. 44 has a very small uncertainty, it is used to calculate the density and compared with the experimental data from Ref. 39. As shown in Fig. 17, the second-order VEOS does not predict the gas density well at temperatures below 15 K. That is because the third and higher virial coefficients become significant at a low temperature and high pressure. At temperatures above 15 K, the VEOS with a second virial coefficient shows good agreement with the experimental data, even at pressures up to 1 MPa. Therefore, it is reasonable to use the above VEOS to check the present EOS at temperatures above 20 K.

Figure 18 shows the calculated density by using the ideal gas equation, the VEOS with the second virial coefficient, and the present EOS. One can also see that the present model agrees with the second-order virial EOS very well, with the maximum deviation of about 0.6%. It indicates that the present model has a good extrapolation performance at temperatures from about 20 K to room temperature, which once again reflects that the EOS developed in the present work is reliable.

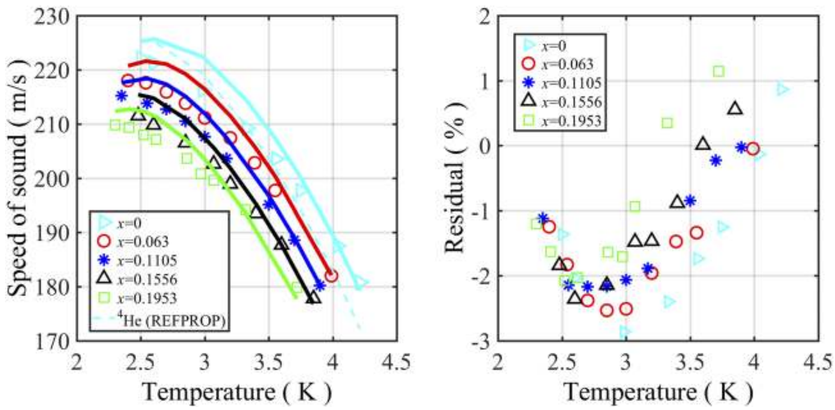

FIG. 16. Comparison of the calculated speed of sound using the KW0 model with the experimental data[49] and its residuals. The solid lines in the left figure are the fitting results.

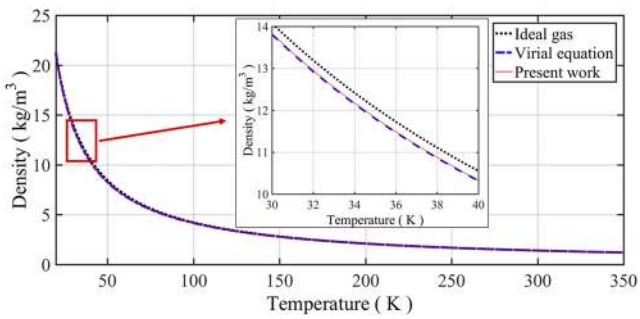

FIG. 18. Comparisons of the present model with the virial EOS and the ideal gas EOS (x = 0.5, p = 1 MPa).

5. Conclusions

The present work developed the first wide-range EOS for ^{3}He–^{4}He mixtures based on the Helmholtz free energy, which is reliable for temperatures from 2.17 K to room temperature and pressures from the vapor pressure to higher than 3 MPa. To obtain an accurate calculation model, four different departure functions from KW0, ^{4}He–Ne, ^{4}He–Ar, and Ne–Ar multi-fluid models were tested. For each of them, five parameters were optimized to find the minimum deviation from the available experimental data by using the Levenberg–Marquardt method. The results showed that the KW0 model was the best one to predict the thermodynamic properties for ^{3}He–^{4}He mixtures.

Comparisons between the present model and the available experimental data show that the present model has a good predictive performance not only for the liquid and gas ρpT relation but also for the VLE properties of ^{3}He–^{4}He mixtures. For most ρpT data, saturated liquid density, and speed of sound, the error of the present EOS is less than 2%. For most data of bubble-point pressure, dew-point pressure, saturated vapor density, and isochoric heat capacity, the error of the present EOS is less than 5%, except for some points near the critical region or the λ-point, the error of which can be higher than 8%. Although the present model gives a relatively poor prediction of the saturated heat capacity, it can be improved in the future if more accurate experimental data are available. Furthermore, by comparing with the virial EOS, it also shows that the current model has good extrapolation performance at temperatures from above 20 K to room temperature.

6. Supplementary Material

The supplementary material contains files with the original data used in the fitting and the database calculated by the present EOS. The calculated tabulated database covers the thermophysical properties of ρpT relation, entropy, enthalpy, heat capacity, volumetric thermal expansion, and compression factor at pressures from saturation up to 3 MPa, temperatures from 2.2 to 350 K, and ^{3}He mole fractions from 0 to 1. In addition, it also includes a calculator developed by using MATLAB graphical user interfaces (GUIs). One can use it to calculate the thermophysical properties at a given point.

Acknowledgments

This work was supported by funding from the European Union's Horizon 2020 research and innovation programme under Marie Skłodowska-Curie Grant Agreement No. 834024 and supported by the National Natural Science Foundation of China (Grant No. 52006231) and the Scientific Instrument Developing Project of the Chinese Academy of Sciences (Grant No. ZDKYYQ20210001).

The authors are grateful to Professor Yonghua Huang from Shanghai Jiao Tong University for providing the software He3Pak for trial. They are also grateful to Professor V. K. Chagovets from the Institute for Low Temperature Physics and Engineering of the National Academy of Sciences of Ukraine for providing the text of Ref. 39. They are also grateful to Dr. Allan Harvey for help and supplying more data for ^{3}He–^{4}He mixtures.

List of Symbols

Abbreviations

^{3}He	helium-3
^{4}He	helium-4
AARD	average absolute relative deviation
EOS	equation of state
KW0	departure function coefficients for hydrocarbon mixtures
VEOS	virial equation of state
VLE	vapor–liquid equilibrium
VPTC	Vuilleumier pulse-tube cryocooler

Symbols

a or A	Helmholtz free energy
C_p	isobaric heat capacity
C_v	isochoric heat capacity
f	fugacity
F_{12}	interaction parameter in departure function
h	enthalpy
k	Boltzmann constant/index of the fitted coefficients
m	mass
N_A	Avogadro constant
N	number of experimental data/number of components in the mixture
p	pressure
R	universal gas constant
T	temperature
u	internal energy/velocity
w	speed of sound
W	weighting coefficients
x	mole fraction vector of mixture constituents
Z	compression factor

Greek letters

α	reduced Helmholtz free energy
α_v	volumetric thermal expansion coefficient
$\beta_{T,12}$, $\gamma_{T,12}$	binary parameters in reducing mixture temperature function

$\beta_{v,12}, \gamma_{v,12}$	binary parameters in reducing mixture density function
δ	reduced density
$\Delta\alpha^{\mathrm{r}}$	departure function
Θ	Debye theta
ρ	density
τ	inverse reduced temperature
φ	fugacity coefficient
χ^2	objective function

Superscript / Subscripts

c	critical value
cal	calculated value
exp	experimental value
i	component index/experimental data index
j	component index
o	ideal part
r	residual part

7. Data Availability

The data that support the findings of this study are available within the article and its supplementary material.

8. Appendix: Conversion of ^{3}He EOS

In the work of Huang *et al.*,[25] the reduced temperature is defined as the inverse of the one used in the common Helmholtz free energy EOS. To use it as the input of our model, the form and its derivative need to be changed. The following equations show those changes for the equations of Huang *et al.*

For reduced Helmholtz free energy,

$$\alpha(\tau,\delta) = \frac{A(1/\tau,\delta)}{RT} = \frac{\tau A(1/\tau,\delta)}{RT_{\mathrm{c}}}.$$

The derivative of reduced Helmholtz free energy is given as follows:

$$\frac{\partial\alpha(\tau,\delta)}{\partial\delta} = \frac{1}{RT}\frac{\partial A(1/\tau,\delta)}{\partial\delta} = \frac{\tau}{RT_{\mathrm{c}}}\frac{\partial A(1/\tau,\delta)}{\partial\delta},$$

$$\frac{\partial^2\alpha(\tau,\delta)}{\partial\delta^2} = \frac{\tau}{RT_{\mathrm{c}}}\frac{\partial^2 A(1/\tau,\delta)}{\partial\delta^2},$$

$$\frac{\partial\alpha(\tau,\delta)}{\partial\tau} = \frac{A(1/\tau,\delta)}{RT_{\mathrm{c}}} - \frac{1}{RT_{\mathrm{c}}\tau}\frac{\partial A(1/\tau,\delta)}{\partial\tau},$$

$$\frac{\partial^2\alpha(\tau,\delta)}{\partial\tau^2} = \frac{1}{RT_{\mathrm{c}}\tau^3}\frac{\partial^2 A(1/\tau,\delta)}{\partial\tau^2},$$

$$\frac{\partial^2\alpha(\tau,\delta)}{\partial\delta\partial\tau} = \frac{1}{RT_{\mathrm{c}}}\frac{\partial A(1/\tau,\delta)}{\partial\delta} - \frac{1}{RT_{\mathrm{c}}\tau}\frac{\partial^2 A(1/\tau,\delta)}{\partial\delta\partial\tau},$$

where A is the Helmholtz free energy in Ref. 25.

9. References

[1] H. Kamerlingh Onnes, in KNAW Proc. **11**, 168 (1909).
[2] D. D. Osheroff, R. C. Richardson, and D. M. Lee, Phys. Rev. Lett. **28**, 885 (1972).
[3] L. D. Landau and I. Ya. Pomeranchuk, Dokl. Akad. Nauk SSSR **59**, 669 (1948).
[4] J. Bardeen, G. Baym, and D. Pines, Phys. Rev. **156**, 207 (1967).
[5] R. Radebaugh, Ň0.6028/NBS.TN.362, 1967.
[6] J. G. M. Kuerten, C. A. M. Castelijns, A. T. A. M. de Waele, and H. M. Gijsman, Cryogenics **25**, 419 (1985).
[7] G. Chaudhry and J. G. Brisson, J. Low Temp. Phys. **155**, 235 (2009).
[8] G. Chaudhry and J. G. Brisson, J. Low Temp. Phys. **158**, 806 (2010).
[9] L. V. Karnatsevich, R. M. Sibileva, M. A. Khazhmuradov, I. N. Shapoval, and A. V. Meriuz, Fiz. Nizk. Temp. **28**, 338 (2002).
[10] R. D. McCarty, J. Phys. Chem. Ref. Data **2**, 923 (1973).
[11] R. M. Sibileva, L. V. Karnatsevich, M. A. Khazhmuradov, and A. V. Meriuz, Low Temp. Phys. **30**, 697 (2004).
[12] A. E. Jahromi and F. K. Miller, Cryogenics **62**, 202 (2014).
[13] B. W. Mueller and F. K. Miller, Cryogenics **79**, 85 (2016).
[14] Z. Zhao and C. Wang, *Cryogenic Engineering and Technologies: Principles and Applications of Cryogen-Free Systems* (CRC Press, USA, 2019).
[15] A. T. A. M. de Waele, Cryogenics **69**, 18 (2015).
[16] A. T. A. M. de Waele, M. Y. Xu, and Y. L. Ju, Physica B **284-288**, 2018 (2000).
[17] J. Wang, C. Pan, T. Zhang, K. Luo, Y. Zhou, and J. Wang, J. Appl. Phys. **123**, 063901 (2018).
[18] N. Jiang, U. Lindemann, F. Giebeler, and G. Thummes, Cryogenics **44**, 809 (2004).
[19] A. Cho, Science **326**, 778 (2009).
[20] H. A. Kierstead, J. Low Temp. Phys. **24**, 497 (1976).
[21] C. Pan, J. Wang, K. Luo, L. Chen, H. Jin, W. Cui, J. Wang, and Y. Zhou, Cryogenics **98**, 71 (2019).
[22] J. Wang, C. Pan, T. Zhang, K. Luo, X. Xi, X. Wu, J. Zheng, L. Chen, J. Wang, Y. Zhou, H. Jin, and W. Cui, Sci. Bull. **64**, 219 (2019).
[23] O. Kunz, R. Klimeck, W. Wagner, and M. Jaeschke, GERG TM15 (Fortschritt-Berichte VDI), VDI Verlag, Düsseldorf, 2007.
[24] O. Kunz and W. Wagner, J. Chem. Eng. Data **57**, 3032 (2012).
[25] Y. Huang, G. Chen, and V. Arp, J. Chem. Phys. **125**, 054505 (2006).
[26] D. O. Ortiz Vega, Ph.D. thesis, Texas A & M University, College Station, TX, 2013.
[27] J. W. Leachman, R. T. Jacobsen, E. W. Lemmon, and S. G. Penoncello, *Thermodynamic Properties of Cryogenic Fluids* (Springer International Publishing, Switzerland, 2017).
[28] B. N. Eselson and N. G. Berezniak, Sov. J. Low Temp. Phys. **3**, 4 (1956).
[29] B. Wallace, Jr. and H. Meyer, Phys. Rev. A **5**, 953 (1972).
[30] B. Wallace, Jr., J. Harris, and H. Meyer, Phys. Rev. A **5**, 964 (1972).
[31] S. G. Sydoriak and T. R. Roberts, Phys. Rev. **118**, 901 (1960).
[32] A. K. Sreedhar and J. G. Daunt, Phys. Rev. **117**, 891 (1960).
[33] R. M. Sibilyova, L. V. Karnatsevich, M. V. Melnykov, and M. A. Khazmuradov, Probl. Atom. Sci. Technol. **44**, 62 (2009).
[34] T. P. Ptukha, Sov. J. Low Temp. Phys. **34**, 7 (1958).
[35] B. N. Eselson, V. G. Ivantsov, P. S. Novikov, and R. I. Shcherbachenko, Ukr. Fiz. Zh. **14**, 1844 (1969).
[36] R. M. Sibilyova, L. V. Karnatsevich, M. V. Melnykov, and M. A. Khazmuradov, Probl. Atom. Sci. Tech. **44**, 103 (2011).
[37] S. Wang, C. Howald, and H. Meyer, J. Low Temp. Phys. **79**, 151 (1990).
[38] I. V. Bogoyavlensky and S. I. Yuechenko, Sov. J. Low Temp. Phys. **2**, 672 (1976).
[39] I. V. Bogoyavlensky, L. V. Karnatsevich, and V. G. Konareva, Fiz. Nizk. Temp. **6**, 1241 (1980).
[40] W. E. Keller, Phys. Rev. **100**, 1021 (1955).
[41] M. A. Barrufet and P. T. Eubank, Fluid Phase Equilib. **35**, 107 (1987).
[42] L. V. Karnatsevich, I. V. Bogoyavlensky, and A. A. Sheinina, Fiz. Nizk. Temp. **14**, 1230 (1988).

[43]J. J. Hurly and M. R. Moldover, J. Res. Natl. Inst. Stand. Technol. **105**, 667 (2000).
[44]W. Cencek, M. Przybytek, J. Komasa, J. B. Mehl, B. Jeziorski, and K. Szalewicz, J. Chem. Phys. **136**, 224303 (2012).
[45]Z. Dokoupil, D. G. Kapadnis, K. Sreeramamurty, and K. W. Taconis, Physica **25**, 1369 (1959).
[46]R. C. Pandorf, E. M. Ifft, and D. O. Edwards, Phys. Rev. **163**, 175 (1967).
[47]J. H. Vignos and H. A. Fairbank, Phys. Rev. **147**, 185 (1966).
[48]T. R. Roberts and S. G. Sydoriak, Phys. Fluids **3**, 895 (1960).
[49]B. N. Eselson, N. E. Dyumin, E. Ya. Rudavsk, and I. A. Serbin, Sov. J. Low Temp. Phys. **6**, 1126 (1967).
[50]D. B. Newell, F. Cabiati, J. Fischer, K. Fujii, S. G. Karshenboim, H. S. Margolis, E. de Mirandés, P. J. Mohr, F. Nez, K. Pachucki, T. J. Quinn, B. N. Taylor, M. Wang, B. M. Wood, and Z. Zhang, Metrologia **55**, L13 (2018).
[51]R. Akasaka, Fluid Phase Equilib. **358**, 98 (2013).
[52]H. Zhang, B. Gao, W. Wu, H. Li, Q. Zhong, Y. Chen, W. Liu, Y. Song, Y. Zhao, X. Dong, M. Gong, E. Luo, and J. Hu, Int. J. Refrig. **89**, 1 (2018).
[53]J. Tkaczuk, I. H. Bell, E. W. Lemmon, N. Luchier, and F. Millet, J. Phys. Chem. Ref. Data **49**, 023101 (2020).
[54]E. W. Lemmon, M. L. Huber, M. O. McLinden, "Reference fluid thermodynamic and transport properties," NIST Standard Reference Database No. 23 Version 9.1, NIST, Boulder, CO, 2013.
[55]See http://www.htess.com/he3pak.htm for He3Pak.
[56]J. Gary, A. O'Gallagher, R. Radebaugh, Y. Huang, and E. Marquardt, REGEN3.3: User Manual, April 2008.
[57]R. Akasaka, J. Therm. Sci. Tech.-Jpn. **3**, 442 (2008).
[58]T. Jindrová and J. Mikyška, Fluid Phase Equilib. **353**, 101 (2013).
[59]J. Gernert, A. Jäger, and R. Span, Fluid Phase Equilib. **375**, 209 (2014).
[60]H. W. Xiang, *The Corresponding-States Principle and Its Practice: Thermodynamic, Transport and Surface Properties of Fluids* (Elsevier Science, Amsterdam, 2005).